Pergamon

Geochimica et Cosmochimica Acta, Vol. 65, No. 8, pp. 1243–1258, 2001

0016-7037/01 $20.00 + .00

PII S0016-7037(00)00601-3

Kinetics, surface chemistry, and structural evolution of microbially mediated sulfide mineral dissolution

MOLLY M. MCGUIRE,[1,*] KATRINA J. EDWARDS,[2] JILLIAN F. BANFIELD,[2] and ROBERT J. HAMERS[1]

[1]Department of Chemistry, 1101 University Ave., Madison, WI 53706, USA
[2]Department of Geology and Geophysics, University of Wisconsin-Madison, 1215 W. Dayton St., Madison, WI 53706, USA

(*Received October* 29, 1999; *accepted in revised form November* 6, 2000)

Abstract—The effects of different microbial populations on the oxidative dissolution of sulfide minerals at 37°C and pH 1.5 were examined over a period of 22 days. Samples of pyrite, marcasite, and arsenopyrite were exposed to a sulfur-oxidizing isolate (*Thiobacillus caldus*), an iron-oxidizing isolate (*Ferroplasma acidarmanus*), and a mixed enrichment culture containing *T. caldus*, *F. acidarmanus*, and *Leptospirillum ferrooxidans*. Changes in chemical speciation of the mineral surface products were monitored by Raman spectroscopy over the course of the experiment, structural evolution was examined with scanning electron microscopy, and the total soluble iron was used as a measure of the dissolution rate.

In the case of all three minerals, an increase in dissolution rate was observed only in the presence of iron-oxidizing microorganisms (i.e., *F. acidarmanus* or the enrichment culture). The chemical speciation at the mineral surface in the presence of these iron-oxidizing species is indistinguishable from that of abiotic control reactions under the same conditions; both are dominated by elemental sulfur. In contrast, experiments with *T. caldus* indicate that the quantity of elemental sulfur on the mineral surface is $<1\%$ of the amount observed on samples exposed to the *F. acidarmanus* culture. It is surprising that removal of the elemental sulfur from the mineral surface by the sulfur-oxidizing species is not accompanied by an increase in the dissolution rate of the mineral. This finding suggests that although elemental sulfur forms on the surface during oxidative dissolution, it does not passivate the mineral surface.

1. INTRODUCTION

The inorganic chemistry of the oxidative dissolution of sulfide minerals and the subsequent generation of acid mine drainage (AMD) have been extensively studied. In particular, the dissolution chemistry of pyrite has been the subject of several comprehensive reviews (Evangelou and Zhang, 1995; Lowson, 1982; Nordstrom, 1982; Nordstrom and Alpers, 1999; Nordstrom and Southam, 1997). Although many of the mechanistic details are still being debated, several facts regarding the overall kinetics have been well established. Ferric iron has been shown to be a more effective oxidant than dissolved oxygen at low pH (Moses et al., 1987), and the rate-limiting step in the oxidation was found to be the regeneration of ferric iron from ferrous iron (Singer and Stumm, 1970). In addition, the surface chemical speciation of pyrite under acidic, oxidative conditions has been examined. A number of surface analysis studies have characterized the mineral surface as "sulfur-rich" and have noted the presence of reaction products such as elemental sulfur and polysulfides (Mycroft et al., 1990; Sasaki et al., 1995; Turcotte et al., 1993). The surfaces of marcasite (Rinker et al., 1997) and arsenopyrite (Buckley and Walker, 1988) also have been found to be enriched in sulfur under acidic, oxidative conditions.

Although the importance of microbial activity in the oxidative dissolution of sulfide minerals is well established, little work has been done to examine the exact role of specific species on the surface composition. Many studies have examined the changes in solution chemistry in the presence of microbial populations (Arkesteyn, 1979; Baldi et al., 1992). Others have investigated the effect of cell attachment on the mineral dissolution rate (Wakao et al., 1984). Only rarely, however, have attempts been made to identify the chemical speciation at the mineral surface during the course of microbially mediated dissolution (Sasaki, 1997; Sasaki et al., 1998b). Without a comparative examination of the chemical changes at the mineral surface, the reaction mechanism itself, as well as the role of various microbial communities on the dissolution of sulfide minerals, cannot be fully understood.

Most laboratory studies of microbial influences on sulfide mineral dissolution have focused on the iron-oxidizing species *Thiobacillus ferrooxidans*. However, in actual acid mine waters, diverse populations of sulfur and iron-oxidizing microorganisms contribute to the dissolution of sulfide minerals (Edwards et al., 1999a; Nordstrom and Southam, 1997; Schrenk et al., 1998). Previous studies have examined mixed cultures of iron and sulfur-oxidizing species and their effects on dissolution rate and generally have found that these mixed microbial populations lead to a significant increase in the rate of dissolution (Battaglia et al., 1994; Curutchet et al., 1996; Edwards et al., 1998; Garcia et al., 1995a;b; Lizama and Suzuki, 1988; Wakao et al., 1982). Most of these laboratory-based studies used microorganisms, such as *T. ferrooxidans* and *Thiobacillus thiooxidans*, which exhibit optimal growth around 25°C and pH 2 to 3. Although these studies have produced important insights into microbial oxidation, many field sites (in particular, sites of acid mine drainage formation) have significantly higher temperatures (often >30°C) and lower pH (often <3) than the conditions where *T. ferrooxidans* and other frequently studied species thrive (Edwards et al., 1999a; Schrenk et al., 1998). In fact, Nordstrom et al. (2000) report negative pH values at the

*Author to whom correspondence should be addressed (mcguire@chem.wisc.edu).

Iron Mountain acid mine drainage site in northern California. The typical solutions draining from this site have pH values of 0.5 to 1.0 and temperatures between 35° and 50°C. In a previous study at this same site, we showed that the distribution of microorganisms varies widely with location. For example, *T. ferrooxidans* is common outside the central mine region where temperatures are lower, but *Leptospirillum ferrooxidans* and several other microbial species dominate at lower pH (Bond et al., 2000a,b; Schrenk et al., 1998). Clearly, understanding such a complex environmental system will require understanding the roles of a large number of microorganisms adapted to specific environments.

In the present study, we examine the effects of several microbial cultures that were isolated from the Iron Mountain site and subsequently cultured in the laboratory. To understand whether microbes with different metabolisms cause characteristic changes in surface reactions, we focused on the effects of an iron-oxidizing isolate, a sulfur-oxidizing isolate, and a mixed culture of iron and sulfur-oxidizing microorganisms on the dissolution rate and surface chemistry of several sulfide minerals. The pH and temperature conditions of the experiment were similar to those encountered at the Iron Mountain field site from which the microorganisms were isolated.

2. EXPERIMENTAL

The experiments described here were designed to evaluate the impact of specific microbial populations on metal sulfide dissolution under conditions relevant to the field site. Microbial species found at the Iron Mountain site were grown to cultures of sufficient size in the laboratory for use in the experiments. Polished mineral samples for surface analyses, as well as ground material that accounted for most of the mineral surface area in each experiment, were thoroughly cleaned beforehand to remove preexisting surface phases. The temperature and pH of the experiments were chosen to match the ranges observed at the field site and the optimal growth conditions of the microbial cultures. Solution aliquots were taken to monitor the total soluble iron concentration as a measure of the rate of reaction and to determine the number of cells suspended in solution. Mineral samples were removed at the same time intervals for determination of surface-attached cell numbers and chemical and structural analysis by Raman spectroscopy and scanning electron microscopy (SEM), respectively.

2.1. Cultures

To help discern whether iron oxidizers and sulfur oxidizers produce surfaces with different chemical compositions, we used isolates of each type as well as an enrichment culture containing a mixed population. All isolates and mixed cultures were obtained from a disused mine at Iron Mountain in northern California (enrichment methods described by Edwards et al., 2000b). The mine site is described elsewhere (Edwards et al., 1999b). Microbial populations included the sulfur-oxidizing bacterium *Thiobacillus caldus* strain TC1 (Edwards et al., 2000a), the iron-oxidizing archaeon *Ferroplasma acidarmanus* strain FER1 (Edwards et al., 2000b), and a mixed enrichment culture grown from sediments and mine water from Iron Mountain. A previous study found that the enrichment culture contains organisms closely related to *Leptospirillum ferrooxidans, F. acidarmanus,* and *T. caldus* (Edwards et al., 2000b). Cultures were grown for one week at 37°C in a sterile medium (Table 1). The media were supplemented with 0.002% yeast extract and adjusted to pH 1.5 with H_2SO_4. The *T. caldus* culture was grown on elemental sulfur (1 g/20 mL) as an energy source. Twenty g/L $FeSO_4 \cdot 7H_2O$ was added to the *F. acidarmanus* during culture growth, and the enrichment culture was supplemented with 2 g/L autoclaved pyrite sediment from the field site. This mineral material was present only during culture growth and was not used for subsequent oxidation experiments. Cells were harvested by centrifugation and washed twice in distilled water adjusted to pH 1.5 with sulfuric acid. The cells then were resuspended in the sterile media without an aqueous energy source.

Table 1. Sterile media.

Compound	mg/L
$(NH_4)_2SO_4$	800
KH_2PO_4	400
$MgSO_4 \cdot 7H_2O$	160
$MnCl_2 \cdot 4H_2O$	0.10
$ZnCl_2$	70
$CoCl_2 \cdot 6H_2O$	0.12
H_3BO_3	31
$Na_2MoO_4 \cdot 2H_2O$	85.2

2.2. Minerals

Research grade pyrite (Spain), marcasite (Indiana), and arsenopyrite (Portugal) samples used in this experiment were purchased from Ward's Natural Science Establishment, Inc. To minimize scattered light that can create a large background signal in Raman spectra, flat mineral surfaces were prepared. Thin polished slabs of pyrite, marcasite, and arsenopyrite were prepared by attaching the minerals to glass slides, cutting thin sections, and then polishing the exposed faces. Although the (001) face of pyrite could be attached directly to the glass slide, it was necessary to first embed marcasite and arsenopyrite samples in epoxy. A diamond saw was used to cut the embedded mineral samples in half, providing large flat faces. For each of the three minerals, slabs $\approx$ 1-mm thick were cut with a sectioning saw after attachment to the glass slides. The exposed faces were polished, and a slow speed wafering saw was used to produce several $\approx 2 \times 2 \times 1$-mm blocks from each slab. The mineral blocks were then removed from the glass slides with acetone and subsequently washed with acetone and ethanol.

For each experiment, several blocks of the appropriate polished mineral were supplemented with crushed mineral to provide sufficient surface area to support growth. In each case, the exposed surface area of the crushed mineral was much greater than the area of the polished mineral blocks; thus, we expect that the overall chemical transformations are controlled by the crushed mineral and are only minimally affected by the polished samples. Crushed minerals were sieved (150–500-μm diameter), ultrasonically treated and washed repeatedly to remove fine particles, and then treated with 10% HCl for 2 h to remove any preexisting oxide layer. The crushed mineral particles then were rinsed with ethanol and allowed to dry. Previous studies have shown that acid-cleaned pyrite samples exhibit reactivity that is similar to that of freshly cleaved samples (Elsetinow et al., 2000).

The surface areas of representative samples of each crushed mineral were analyzed with a BET Surface Area Analyzer (Quantachrome Corp.) and were found to be $(2.30 \pm 0.02) \times 10^{-2}$, $(2.70 \pm 0.08) \times 10^{-2}$, and $(1.6 \pm 0.09) \times 10^{-2}$ m^2/g for pyrite, marcasite, and arsenopyrite, respectively, where each error represents the standard deviation of triplicate analyses. Pyrite (2.002 g), 1.747 g of marcasite, or 2.870 g of arsenopyrite were added to each flask to ensure equal starting surface areas of 4.7×10^{-2} m^2 per experiment. Flasks (250 mL) were sterilized by autoclaving at 126°C and 20 psi for 20 min and then for an additional 8 min after the addition of the mineral material. The brevity of the autoclaving process minimized oxidation of the mineral material before the start of the laboratory experiments.

2.3. Laboratory Oxidation Experiments

Twenty-four separate experiments were conducted, including duplicate runs of each of the possible combinations of the four microbial environments (the three different cultures and an abiotic control) and the three sulfide minerals. In the experiments with microbial populations, 35 mL of pure media and 5 mL of media containing resuspended cells were added to the flask containing the crushed mineral material and 12 mineral blocks. In the abiotic control experiments, 40 mL of media were added to each flask. All reaction vessels were maintained

Table 2. Surface area normalized dissolution rates and calculated errors.

	Dissolution rate (μmol/m^2/d)		
	Pyrite	Marcasite	Arsenopyrite
T. caldus	100 ± 20	200 ± 30	380 ± 120
F. acidarmanus	150 ± 10	320 ± 100	980 ± 150
Enrichment culture	230 ± 30	1000 ± 330	1330 ± 360
Abiotic control	100 ± 20	250 ± 80	510 ± 110

at 37°C for the duration of the experiment after addition of the media. Mineral blocks were removed from each reaction flask with autoclaved forceps at 2, 5, 10, 15, and 22 days for chemical analysis by Raman spectroscopy, structural analysis by SEM, and determination of cell counts.

2.4. Iron Analyses

Solution aliquots of 1.5 mL were taken at the start of the experiment and thereafter concurrently with removal of mineral samples for surface analysis. Cells and particulate matter were removed from the aliquots by centrifugation. Total soluble iron concentrations were determined by using the ferrozine method of Dawson and Lyle (1990). Spectrophotometric analysis was performed with a Perkin Elmer Lambda 20 UV-vis spectrophotometer. Total iron concentrations were averaged for the duplicate experiments. The iron analyses for one of the experiments involving marcasite with the *F. acidarmanus* culture showed erroneous iron concentrations near the detection limit of the method. The measurements reported in this case were obtained from only one run and do not represent an average of the two duplicate reactions.

Average dissolution rates, as quoted in Table 2, are the slopes of the best straight-line fit to the averaged iron concentrations using the method of least squares. Confidence intervals for the slopes were calculated at the 95% confidence level. The data point for arsenopyrite in the *F. acidarmanus* culture at 22 days was a statistical outlier based on the slope calculated from the other points and was subsequently removed from the data set.

2.5. Cell Counts

Cells counts were determined for cells suspended in aqueous solution and also for those attached to the mineral surfaces. The aqueous aliquots (1.5 mL) taken at 2, 5, 10, 15, and 22 days were analyzed by using a hemocytometer. The number of cells attached to mineral surfaces was estimated by examining one polished mineral block at each sampling interval. The block was fixed in 4% paraformaldehyde in phosphate-buffered saline (PBS) buffer (0.137 mol/L NaCl, 0.005 mol/L $NaHPO_4 \cdot 7\ H_2O$, 0.003 mol/L KCl, 0.001 mol/L KH_2PO_4) at pH 7.3 for 2 h. The samples were then rinsed with ethanol and stained with 4′,6-diamidino-2-phenylindole (DAPI) (Kapuscinski, 1995) before examination by ultraviolet (UV) epifluorescent microscopy using a Leica LEITZ DMRX microscope. Images were captured with a charge-coupled device and analyzed with Scion Image Analysis software. Depending on cell densities and a subjective estimation of colonization heterogeneity, 2 to 12 images (72 × 95.75 μm) were averaged to determine cell density on each mineral sample.

2.6. Fluorescent In Situ Hybridizations (FISH)

To determine the relative proportion of the sulfur-oxidizing *T. caldus* in the enrichment culture, an oligonucleotide probe specific for the *T. caldus* bacteria species (Edwards et al., 2000a) was used to identify these microorganisms on select samples. Polished mineral blocks were examined at 15 days, whereas cells suspended in aqueous solution were examined in the initial inoculum and at the end of the experiment. Samples were fixed in 4% paraformaldehyde in PBS buffer (0.137 mol/L NaCl, 0.005 mol/L $NaHPO_4 \cdot 7\ H_2O$, 0.003 mol/L KCl, 0.001 mol/L KH_2PO_4) at pH 7.3 for 2 h. Hybridization of the fixed samples on glass slides (for the aqueous suspensions) or mineral surfaces was performed in a buffer containing 0.9 mol/L NaCl, 20 mM Tris/HCl (pH 7.4), 0.01% sodium dodecyl sulfate (SDS), 25 to 50 ng of oligonucleotide probe, and 25% formamide. The samples were incubated in a buffer-equilibrated humidity chamber at 46°C for 90 min, rinsed briefly, and then immersed in a wash buffer consisting of 20 mM Tris/HCl (pH 7.4), 0.01% SDS, 5 mM EDTA, and between 7 mM and 0.9 mol/L NaCl. The NaCl content of the wash buffer was calculated to achieve the same stringency as the hybridization buffer according to the formula of Lathe (1985). Finally, samples were rinsed with distilled water, air dried, and mounted with Vectashield (Vector Laboratories) before examination by UV epifluorescent microscopy. The number of iron oxidizers in the enrichment culture was taken as the difference between the total cell counts as determined by DAPI staining and the number of sulfur-oxidizing cells hybridized by the *T. caldus* probe.

2.7. Raman Spectroscopy

Mineral samples to be analyzed by Raman spectroscopy were rinsed in deionized water after removal from the reaction vessels. All samples were analyzed within 12 h after removal from solution. The Raman detection system consisted of a high-throughput f/1.8 spectrograph from Kaiser Optical Systems with a fixed resolution of ≈2 cm^{-1} and a liquid nitrogen-cooled charge coupled device (CCD) detector from Photometrics. Data were collected on a PC with the MAPS spectral data acquisition program (Photometrics). An Ar ion laser (Omnichrome) operating at 514 nm and ≈10 mW power was used as the illumination source. The CCD array permitted use of a low-power laser, thereby reducing any possibility of photochemical changes or volatilization induced by the incident illumination. Acquisition times varied from 2 to 30 min total, depending on the signal-to-noise ratio. Each spectrum was the result of addition of several shorter acquisitions that were individually analyzed for cosmic ray spikes. The acquisition region extended from 100 to 2500 cm^{-1}, but no features were observed beyond 1200 cm^{-1}. Except where noted, the spectra in each figure have been normalized to the signal from the bulk mineral to approximately correct for changes in optical alignment and provide a common reference point.

A standard for quantitative calibration of the Raman signal of elemental sulfur consisted of a known quantity of elemental sulfur on a pyrite sample. A 3-μL of 3.3 × 10^{-2} M elemental sulfur in carbon disulfide was placed on the polished pyrite surface. After evaporation of the solvent, the area of the spot left on the pyrite surface was measured and estimated to be 6.3 × 10^{-2} cm^2. The resultant surface coverage of the calibration standard was ≈10^{18} mol/cm^2. Because drying occurs in a very heterogeneous manner, this method serves only as a crude standard, but it suffices to give a rough estimate of the sulfur layer thickness. More quantitative analyses using solution-phase methods (McGuire and Hamers, 2000) confirm the validity of this rough calibration.

2.8. Electron Microscopy

SEM was used to examine the structural morphology of polished mineral blocks throughout the course of the experiments. Samples were carbon coated after fluorescent microscopy analysis and then examined with a LEO DSM-982 Field Emission SEM microscope operated at 3 kV. Energy-dispersive X-ray (EDX) analysis was used for elemental analysis of secondary mineralization.

3. RESULTS

3.1. Raman Spectra

The Raman spectrum of clean, unreacted arsenopyrite is shown in Figure 1. The arsenopyrite peaks are noted at 129, 169, 192, 304, 332, and 407 cm^{-1}. This spectrum is substantially different from that of the only other spectrum found in the literature (Mernagh and Trudu, 1993). X-ray diffraction analysis (data not shown) confirmed the identity of our samples as arsenopyrite.

Figure 2 illustrates the series of Raman spectra obtained after

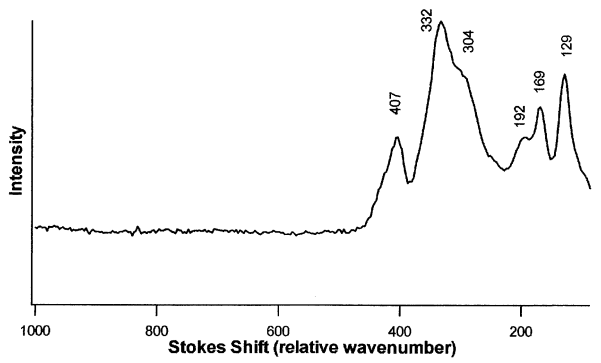

Fig. 1. Raman spectrum of unreacted arsenopyrite. Sample was polished and treated with 50% HCl for 2 h.

various reaction times for marcasite (2a), arsenopyrite (2b), and pyrite (2c) in the abiotic control experiments. Marcasite appears at 323 and 387 cm^{-1} (Mernagh and Trudu, 1993), whereas bulk pyrite gives rise to the three peaks at 342, 378, and 428 cm^{-1} (Ushioda, 1972). Another common feature in the Raman data is the set of three peaks at ≈822, 869, and 931 cm^{-1} that are most easily seen in Figure 2b in the arsenopyrite spectrum after reaction for 22 days. These three peaks have been assigned to silicate (SiO_4) inclusions that are known to occur within these sulfide minerals (Chopelas, 1991).

Over the course of the experiment, the most notable change in the Raman spectra is the appearance of new, sharp peaks at approximately 470, 432, 244, 217, and 151 cm^{-1} as indicated in the marcasite spectrum at the top of Figure 2a. We attribute these spectral features to the vibrational modes of elemental sulfur (Mycroft et al., 1990). The same peaks can be seen in the spectrum of the sulfur standard in Figure 7a. The elemental sulfur peaks predominate in the spectra of both arsenopyrite and marcasite over the entire course of the reaction. The relative abundance of sulfur on these surfaces (as noted by the peak heights in the normalized spectra of each set) is variable from sample to sample, but it is the major spectral feature observed for both marcasite and arsenopyrite. In contrast, the pyrite spectra show little evidence of elemental sulfur over 22 days.

To examine the effect of individual microbial species on the surface chemistry, Raman spectroscopic studies were performed on mineral samples exposed to each of the isolates. Figure 3 presents the spectra of marcasite (3a), arsenopyrite (3b), and pyrite (3c) surfaces that were exposed to the *F. acidarmanus* population over the course of the experiment. The Raman spectra of the mineral samples exposed to the iron-oxidizing *F. acidarmanus* are similar to those observed in the abiotic control experiments. Strong spectral signatures of sulfur are observed on marcasite and arsenopyrite, whereas very little evidence for the presence of sulfur is detected on the pyrite surfaces. Several other features appear in the pyrite spectra, including the large peak at ≈600 cm^{-1} observed in the spectra of the samples exposed for 10 and 22 days. Although we have been unable to assign these features to a particular bulk or surface phase, we have been able to rule out common iron sulfate compounds based on the absence of additional strong peaks that appear at ≈430, 300, and 220 cm^{-1} in the Raman spectra of jarosite-group compounds [$MFe_3(SO_4)_2(OH)_6$, $M^+ = K^+$, NH_4^+, Na^+, Ag^+, and $1/2Pb^{2+}$] (Sasaki et al., 1998a). Other sulfoxy anions, such as sulfate or thiosulfate, can be ruled out as well on the basis of the absence of S-O stretches that would be expected to appear near 1000 cm^{-1} (Sato et al., 1985). Although iron oxide species, such as hematite or goethite, might be anticipated surface products because of the high iron concentrations, the absence of an additional intense spectral feature near 400 cm^{-1} rules out these compounds as possible surface phases (Thibeau et al., 1978).

Figure 4 reveals that the minerals in contact with *T. caldus* populations exhibit very different spectra from those exposed to the *F. acidarmanus* culture. Particularly striking is that the Raman spectra of samples exposed to the *T. caldus* culture show little evidence for elemental sulfur, with the exception of one arsenopyrite sample. In fact, the spectra of *T. caldus*-exposed samples closely resemble those of the clean, unreacted samples, and no additional spectral features are observed. Figure 5 is an expansion of a portion of the spectrum of marcasite after 15 days in the *T. caldus* culture. The arrows in the figures indicate the expected peak positions for the three most intense elemental sulfur peaks. Although the spectrum is sufficiently magnified vertically to reveal the noise, elemental sulfur is not observed on this scale. Using the noise level as an upper limit to the amount of elemental sulfur on the *T. caldus*-exposed samples and quantitatively comparing the peak intensities, we can establish that the amount of residual sulfur observed in the presence of *T. caldus* is $<1\%$ of the sulfur present on the samples exposed to the *F. acidarmanus* culture.

Figure 6 illustrates the Raman spectrum for each mineral in the presence of the enrichment culture containing *F. acidarmanus*, *T. caldus*, and *L. ferrooxidans*. The influence of a mixed population of iron oxidizers and sulfur oxidizers was studied to determine whether the observed effects are accounted for by the simple addition of the contributions from each of the isolates. The new features observed in these spectra are similar to those observed in the experiments with the iron-oxidizing isolate. The dominant lines in the spectra are assigned to the vibrational modes of elemental sulfur. However, it is surprising that several of the spectra of pyrite exposed to the enrichment culture possess a sulfur signal of comparable intensity to the sulfur signal of the marcasite and arsenopyrite samples.

3.2. Quantification of Sulfur Coverage

The abundance of elemental sulfur on the various mineral surfaces was quantified roughly by calibrating the Raman intensities with a standard of known coverage. By assuming a surface density of $\approx 10^{15}$ mol/cm^2 for bulk elemental sulfur, the calibration standard in this case corresponds to a surface coverage of elemental sulfur on the order of a thousand monolayers. Although the evaporation of the solvent from the droplet on the mineral surface produces substantial heterogeneity in the lateral concentration of deposited solutes, the standard suffices as a crude estimate of the sulfur coverage.

Figure 7 illustrates a comparison between the spectra of the calibration standard (7a), a marcasite sample after 10 days of reaction in the iron-oxidizing isolate (7b), and a pyrite sample after 22 days in the iron-oxidizing isolate (7c,d). The marcasite sample serves as a representative example of typical sulfur intensities observed in these experiments. Because pyrite and

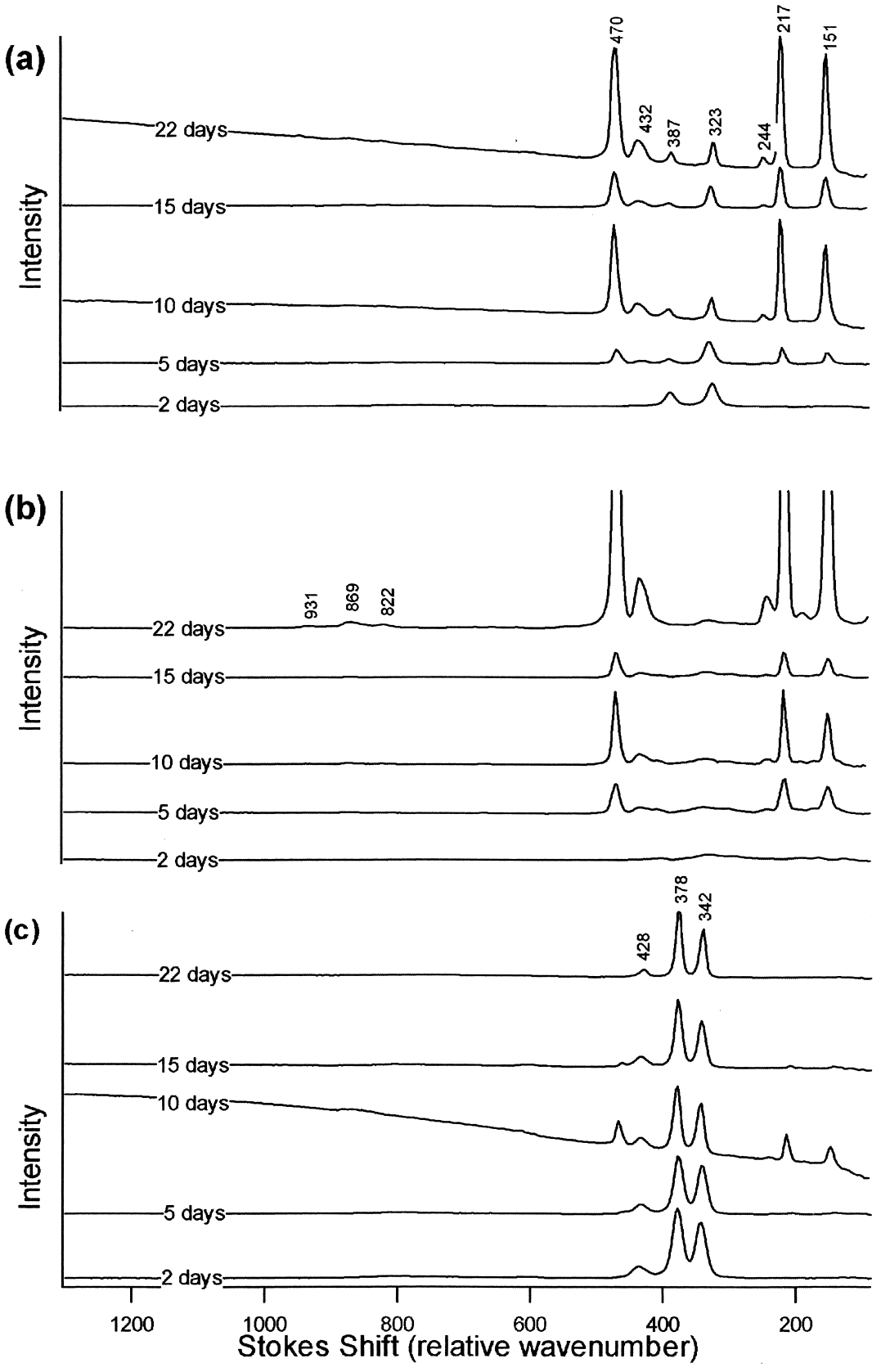

Fig. 2. Raman spectra of marcasite (a), arsenopyrite (b), and pyrite (c) after reaction in the abiotic media at pH 1.5 and 37°C. Spectra of each mineral are approximately normalized to the signal from the bulk mineral. Time labels indicate number of days of reaction.

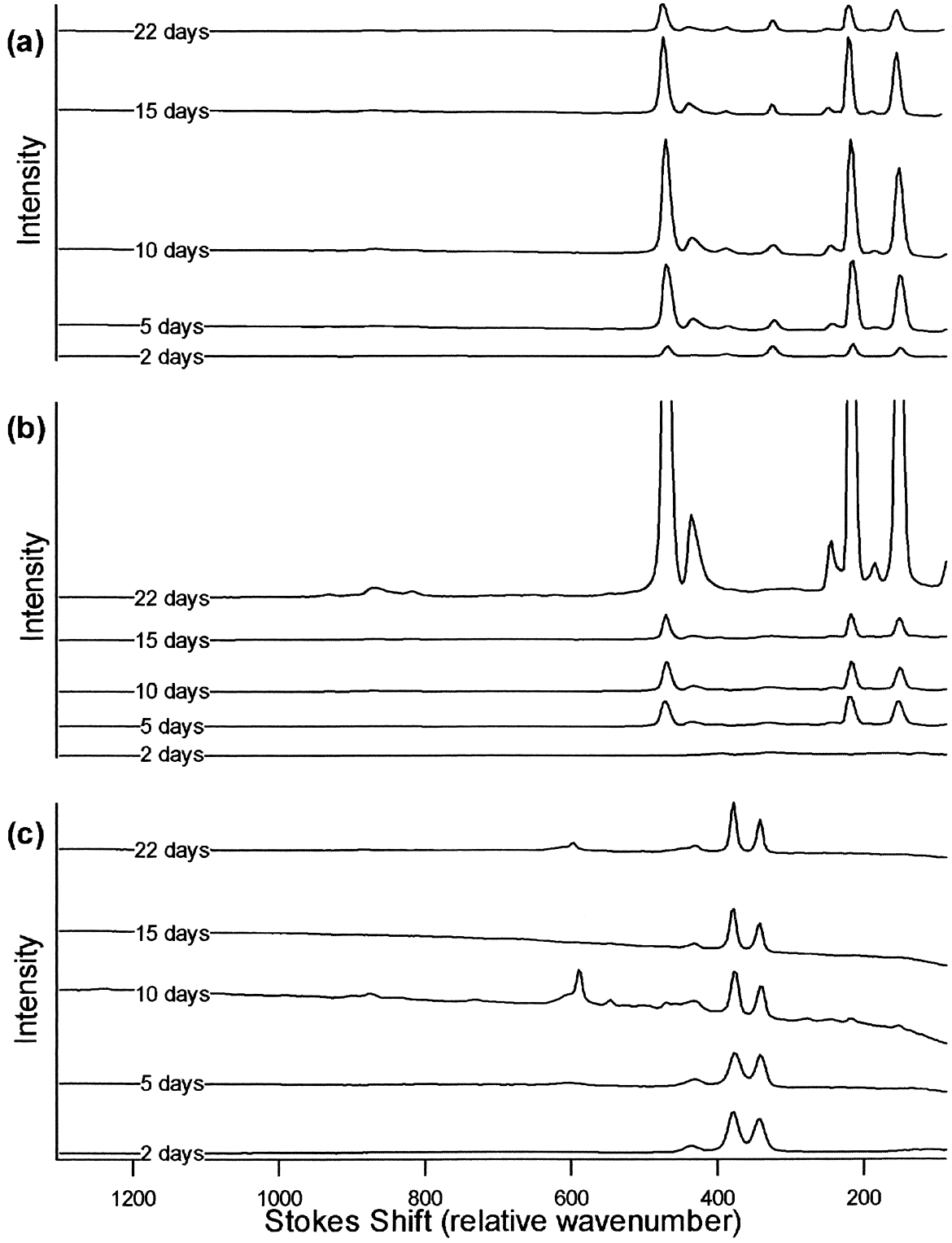

Fig. 3. Raman spectra of marcasite (a), arsenopyrite (b), and pyrite (c) after reaction in the *F. acidarmanus* culture at pH 1.5 and 37°C. Spectra of each mineral are approximately normalized to the signal from the bulk mineral. Time labels indicate number of days of reaction.

marcasite are observed to have comparable Raman sensitivities, the intensities of the sulfur peaks normalized to the bulk for the spectra of the standard and the marcasite sample suggest that the two have approximately equal coverages of elemental sulfur.

The pyrite sample from the end of the reaction period,

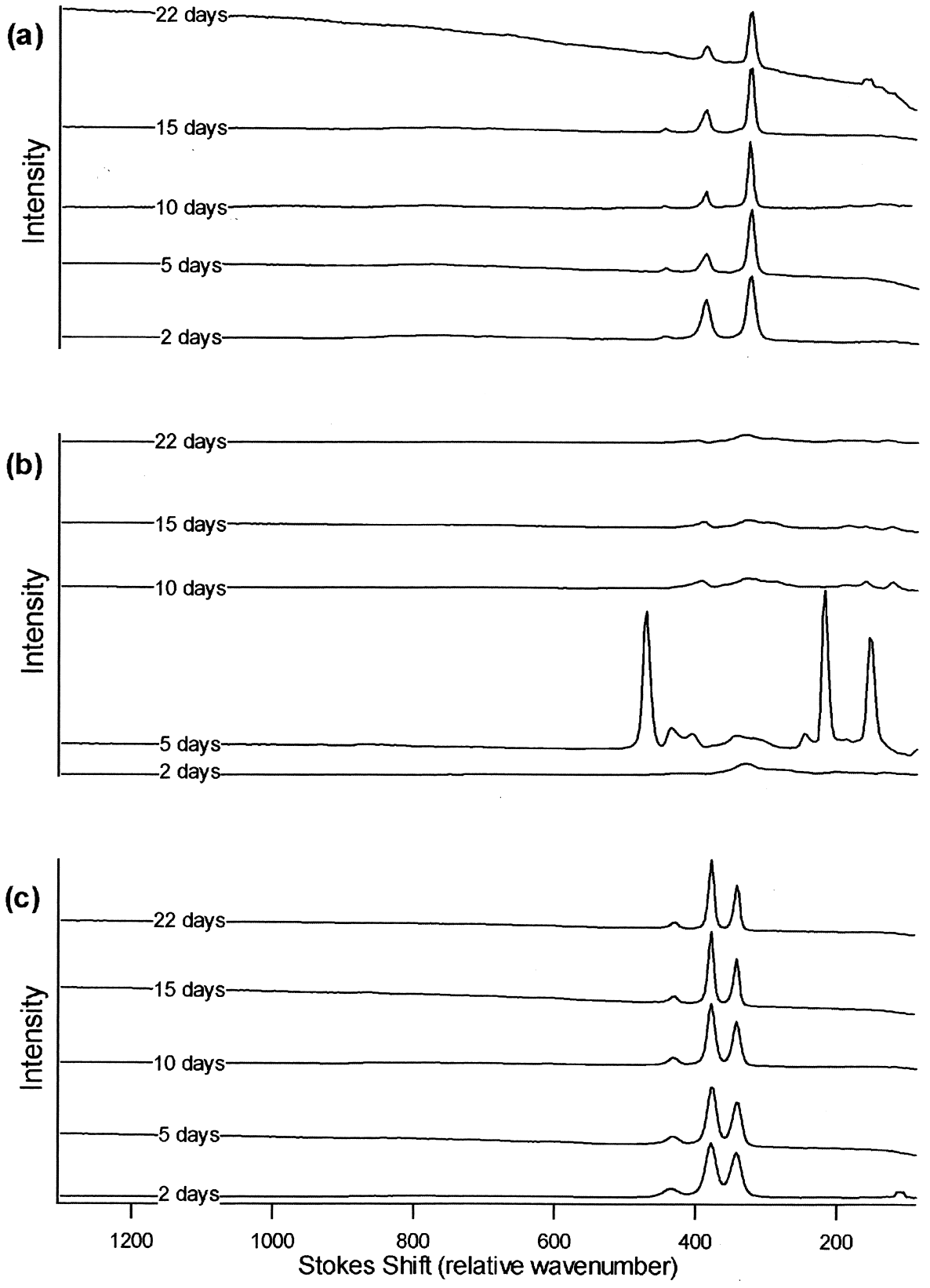

Fig. 4. Raman spectra of marcasite (a), arsenopyrite (b), and pyrite (c) after reaction in the *T. Caldus* culture at pH 1.5 and 37°C. Spectra of each mineral are approximately normalized to the signal from the bulk mineral. Time labels indicate number of days of reaction.

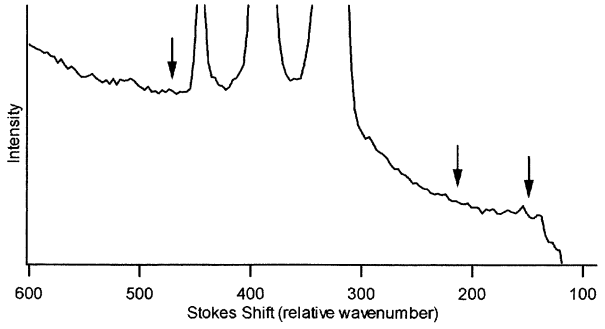

Fig. 5. Raman spectrum of marcasite after 15 days of reaction in the *T. caldus* culture at pH 1.5 and 37°C. The vertical scale of the plot has been expanded to show the noise level in the spectrum. The arrows mark the expected positions of the three most intense Raman lines from elemental sulfur.

however, reveals little evidence for the formation of elemental sulfur. The inset (7d) is an expanded view of a portion of the pyrite spectrum from Figure 7c. Small peaks due to sulfur, barely distinguishable from the noise, are visible. The rough calibration procedure allows us to establish that, in this case, the peak intensities correspond to a sulfur coverage of no more than a few monolayers.

3.3. Structural Homogeneity

Representative SEM images from abiotically reacted minerals are shown in Figure 8. Under abiotic conditions, pyrite samples were not heavily etched and evidenced very little secondary mineralization (Fig. 8a). Marcasite and arsenopyrite, in contrast, both exhibited linear dissolution features (Fig. 8b) and secondary mineralization, often in the form of large ($>$20 μm in diameter) deposits (Fig. 8c). Energy-dispersive X-ray (EDX) spot analyses (data not shown) indicated that these deposits were enriched in sulfur relative to the underlying mineral.

As illustrated in Figure 9, SEM images of the three minerals exposed to *T. caldus* revealed patterns of pitting and surface roughening similar to those exhibited by their counterparts in the abiotic control experiments. However, in the presence of the sulfur-oxidizing *T. caldus,* the large sulfur-rich deposits observed on arsenopyrite and marcasite in the abiotic controls were absent (Fig. 9b,c). In addition, zones of secondary mineral depletion surrounding cells were seen (Fig. 9c).

The evolution of the surface morphology resulting from exposure to either *F. acidarmanus* or the enrichment culture was very distinct from that resulting from exposure to *T. caldus.* As seen in Figure 10a, pyrite exhibited heterogeneous dissolution patterns resulting in discrete pits 5 to 50 μm in diameter on some surfaces. Pit size, distribution, and number density varied considerably between samples and often were localized by inclusions. Both marcasite and arsenopyrite surfaces developed pronounced surface roughening (Fig. 10b,c) and linear dissolution features (Fig. 10b) in the presence of either *F. acidarmanus* or the enrichment culture but did not form the discrete euhedral dissolution pits observed on pyrite. In addition, large sulfur-rich deposits, similar to those observed on the abiotic control samples, were apparent on both marcasite and arsenopyrite surfaces (Fig. 10b,c).

3.4. Analysis of Chemical Homogeneity

Although SEM provides useful information on the structural morphology of the mineral surfaces, it may not provide an accurate representation of the spatial distribution of elemental sulfur on the mineral surface. Mycroft et al. (1990) reported that sulfur deposits on pyrite surfaces often were observed to vanish within minutes when examined by SEM/EDX, presumably because the intense electron beam leads to local heating and volatilization of sulfur. Raman spectroscopic analysis at low laser powers under ambient conditions does not present the same dangers of modification of the mineral surface. To obtain a more accurate description of the distribution of elemental sulfur on the mineral surfaces, the imaging function of the CCD array detector was used to analyze the spatial variation of the Raman signals. Analyses were performed on a marcasite sample reacted for 22 days in a duplicate abiotic control experiment at pH = 1.5 and 37°C. Rather than focusing the incident light to a point, the beam was focused to a line $\approx$ 3 mm in length and several hundred microns wide. The scattered light from this excitation region was then imaged across the vertical extent of the CCD detector. When the detector is operated in imaging mode, the horizontal axis gives spectral information, but the vertical axis of the CCD gives a one-dimensional spatial profile of the Raman intensity along the mineral surface with a spatial resolution determined by the size of the CCD array elements, 25 μm. By dissecting the two-dimensional image into horizontal bands, a series of spectra, each representing a different area of the surface, were obtained.

The marcasite image obtained in this fashion was analyzed statistically in horizontal bands that corresponded roughly to the sample area probed when the incident light is focused to a point rather than a line. An averaged spectrum for each band was generated, and the intensity of the elemental sulfur signal at 432 cm^{-1} normalized to the bulk marcasite peak at 323 cm^{-1} was calculated for each of the horizontal strips. Our analysis of the Raman images obtained in this way indicates that the bulk-normalized sulfur intensity obtained over different regions of the surface of a typical sample has a statistical fluctuation of 15%. This value is also consistent with the variations observed in less systematic studies of the intensities at various locations using a circular focal spot. The spatial distribution of the elemental sulfur has been further confirmed in preliminary studies of sulfide mineral surfaces using imaging Raman spectroscopy with a spatial resolution of $\approx$3 μm (McGuire et al., in review). Consequently, we conclude that although the surface products are indeed distributed heterogeneously across the sample, the sampling area in our experiments is sufficiently large that these inhomogeneities lead to only a small ($\approx$15%) variation in the normalized intensities. This uncertainty is sufficiently small that the conventional (nonimaging) spectra are representative for the purposes of this study.

3.5. Rates of Dissolution

The change in total soluble iron as a function of time was monitored as a measure of the dissolution rate for each of the

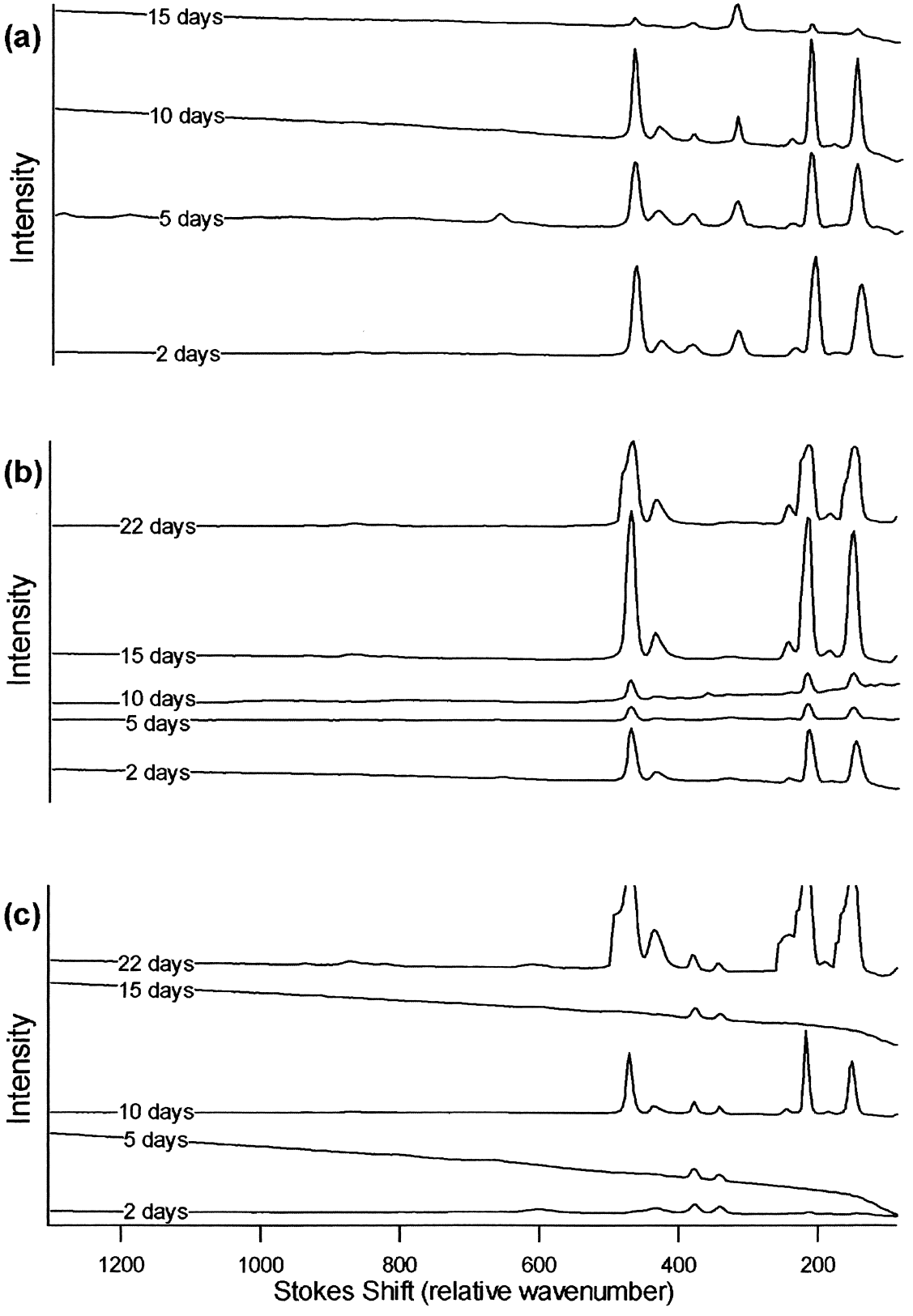

Fig. 6. Raman spectra of marcasite (a), arsenopyrite (b), and pyrite (c) after reaction in the enrichment culture at pH 1.5 and 37°C. Spectra of each mineral are approximately normalized to the signal from the bulk mineral. Time labels indicate number of days of reaction.

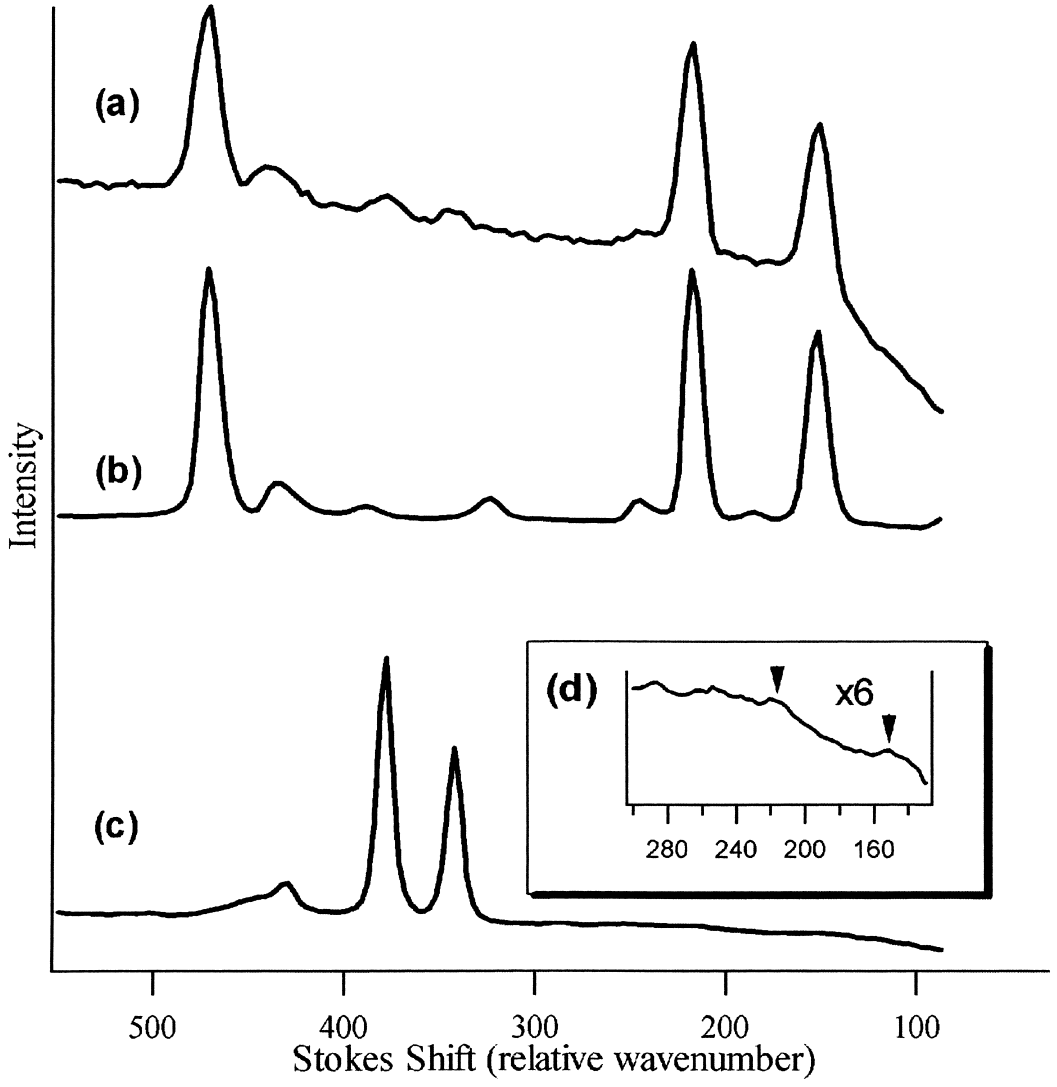

Fig. 7. Raman spectra of the sulfur calibration standard (a), marcasite after 10 days in the *F. acidarmanus* culture (b), pyrite after 22 days in the *F. acidarmanus* culture (c). All reactions were at pH 1.5 and 37°C. The pyrite spectrum is enlarged by a factor of 10 compared with the marcasite sample. The inset (d) shows a further expansion (×6) of the pyrite spectrum in the region of 140 to 300 cm^{-1}. The arrows indicate the expected peak positions for two strong elemental sulfur lines in this region.

minerals. Although the high iron concentrations in some of the experiments suggest the possibility of precipitation of iron-bearing minerals, the rate data suggest that such a process is not playing a major role in the dissolution. A decrease in the reaction rate over time would be evident if iron-consuming pathways were depleting the concentration of iron in solution. The iron concentrations continue to increase linearly over the course of reaction. Thus, we believe that the total iron concentration of the solutions is a valid measure of the mineral dissolution rate. Although the rates of dissolution would be expected to change throughout the course of each experiment as the chemical and microbial conditions evolve (McKibben and Barnes, 1986), no statistically significant deviations from a linear increase in total Fe concentration were observed. Consequently, the slopes were used as a measure of the dissolution rate.

The rate data presented in Figures 11 to 14 as the total number of moles of iron released per unit mineral surface area have been fitted with a straight line to yield an average dissolution rate. The surface-area normalized dissolution rates for each experiment and the calculated error associated with the line fit are summarized in Table 2. No attempt was made to force the linear fits to pass through the origin. Although almost all of the fits passed through zero within the experimental error, some non-zero intercepts were observed. These non-zero intercepts could be the result of an induction period at the beginning of a surface-controlled reaction, during which either reaction is initially fast because sites of high reactivity are consumed quickly before the surface reaches a steady-state structure, or reaction is slow to initiate because only sites of low reactivity are available during the initial period of the reaction (Hirth and Pound, 1963). The first process would result in a positive

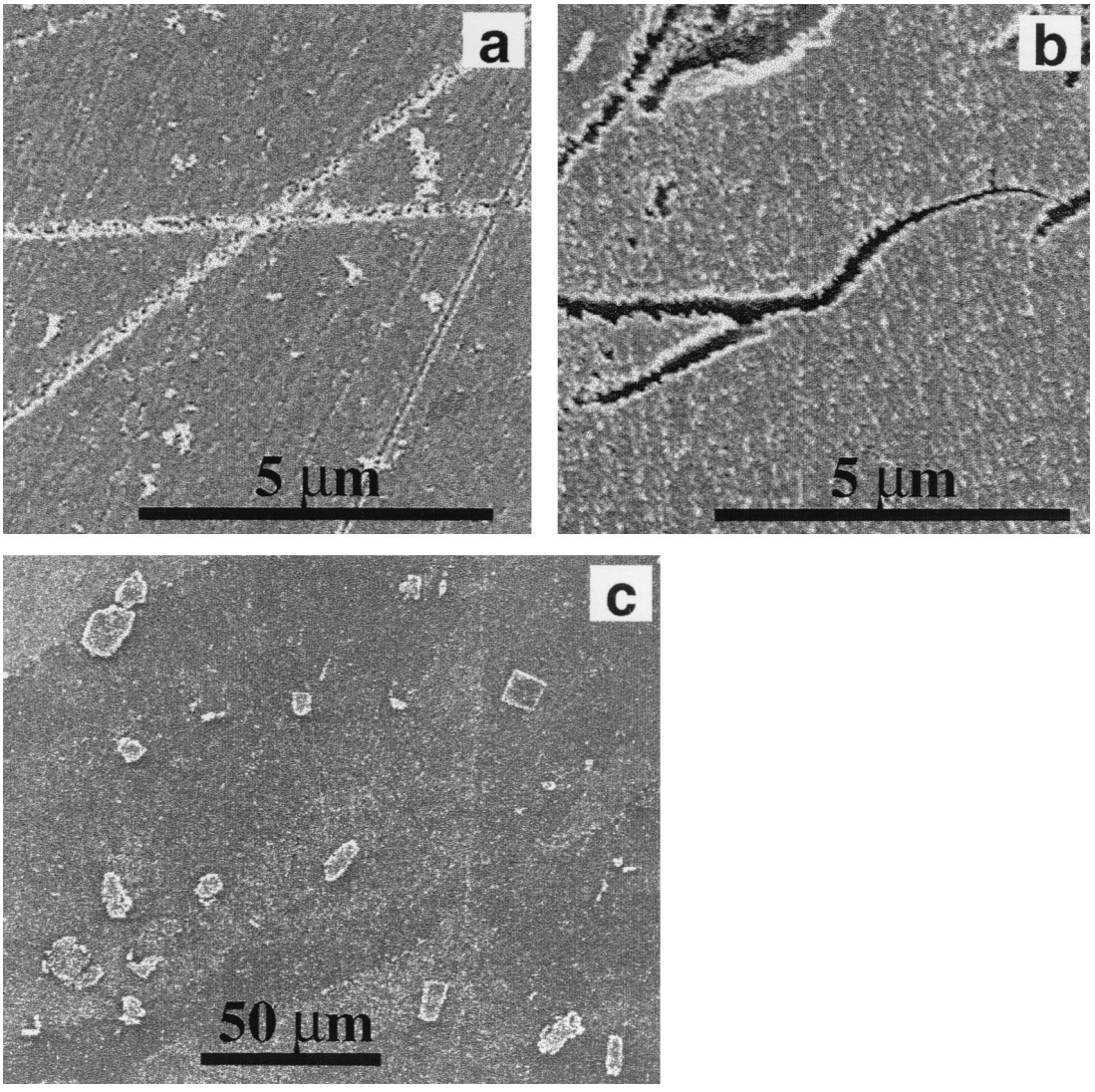

Fig. 8. SEM images of pyrite (a), marcasite (b), and arsenopyrite (c) after 22 days of reaction in the abiotic media at pH 1.5 and 37°C.

intercept, whereas the second would lead to a negative intercept.

Figure 11 shows the total soluble iron as a function of time for each of the minerals in the abiotic control at pH 1.5. The three sulfide minerals exhibited pronounced differences in reactivity. The data indicate that the pyrite dissolution rate is approximately half of the marcasite rate and one fifth of the arsenopyrite dissolution rate. Similar trends are apparent in the experiments with microbial populations as well.

Figure 12 compares the dissolution rates of arsenopyrite in the different media. This comparison reveals the effect of each type of microbial population on the reaction rate. Arsenopyrite exposed to the sulfur-oxidizing *T. caldus* shows no statistically significant difference in rate compared with the control. In contrast, the iron-oxidizing *F. acidarmanus* and the enrichment culture exhibit dissolution rates that are ≈2 and 2.5 times higher than the abiotic control, respectively.

Figure 13 illustrates the rate data for marcasite in each of the four environments. In the case of marcasite, neither the *T. caldus* nor the *F. acidarmanus* culture exhibited a rate significantly different from the abiotic control. Only in the presence of the enrichment culture did marcasite reveal a significant (approximately fourfold) increase in the rate of dissolution.

Total soluble iron vs. time for pyrite in each environment is shown in Figure 14. Again, the rate in the presence of *T. caldus* was approximately equal to the rate of the abiotic control. The enrichment culture produced a twofold increase in the dissolution rate, whereas the iron-oxidizing *F. acidarmanus* increased the rate by a factor of 1.5.

3.6. Cell Counts

Average total cell counts for each experiment, as well as the proportion of iron-oxidizing cells in the enrichment culture are presented in Table 3. Although cell numbers varied by over an order of magnitude during each experiment (data not shown), average cell counts were on the order of 10^9 for all experiments.

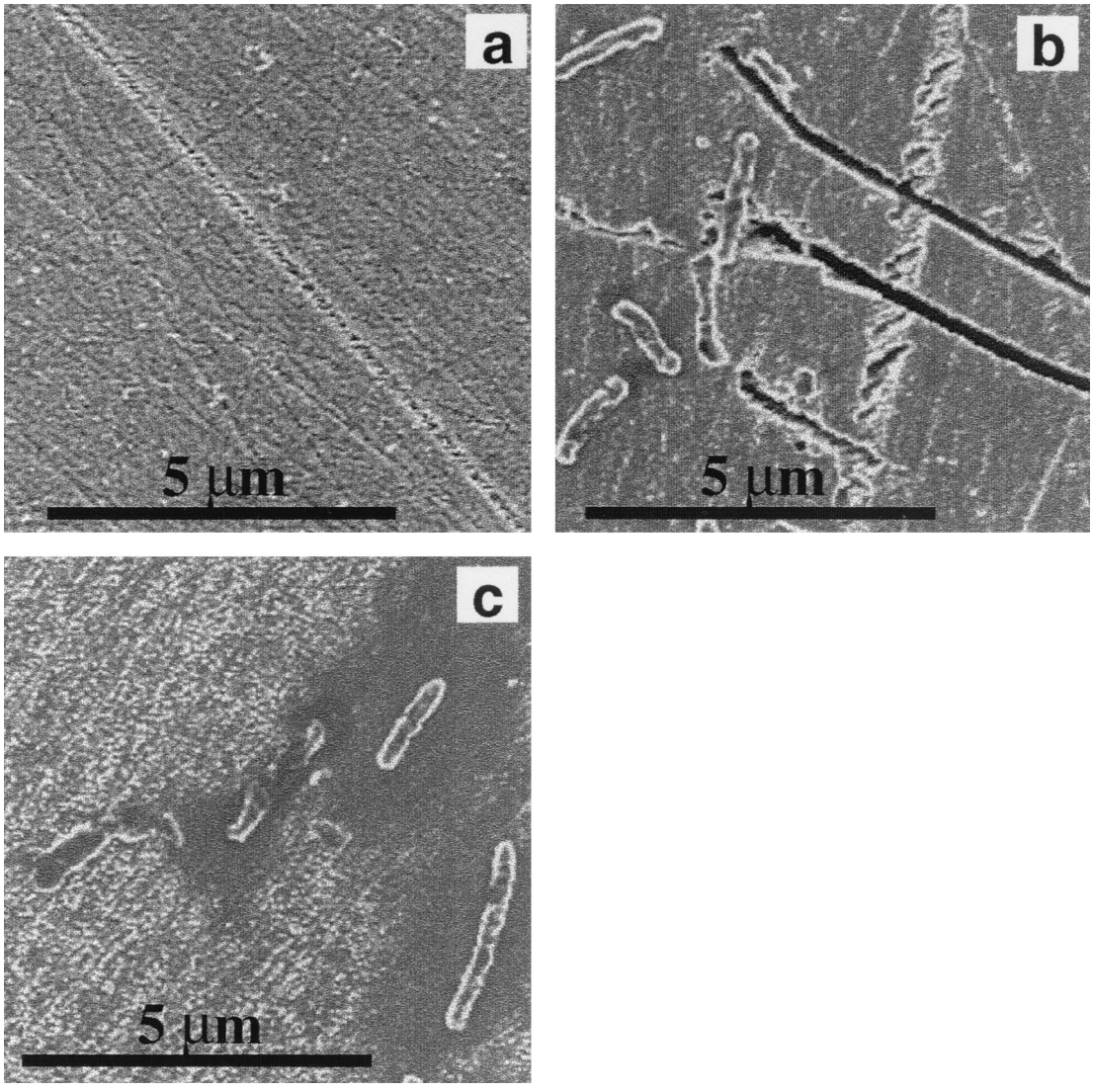

Fig. 9. SEM images of pyrite (a), marcasite (b), and arsenopyrite (c) after 22 days reaction in the *T. caldus* culture at pH 1.5 and 37°C.

4. DISCUSSION

4.1. Comparison of Microbially Mediated Dissolution and Abiotic Dissolution

The minerals exposed to the *F. acidarmanus* culture and the enrichment culture, as well as those reacted in the abiotic medium, exhibit a similar buildup of elemental sulfur at the surface. This observation is not surprising because elemental sulfur is insoluble in acidic solutions. In contrast, other possible oxidation products, such as sulfates and iron oxides, would be very soluble in an aqueous solution at pH 1.5, and therefore, would not be expected to form deposits more than one atomic layer in thickness.

The similarity of the surface products in the abiotic media and the iron-oxidizing microbial cultures is not at odds with the observed differences in dissolution rate between the experiments. If the rate of dissolution is dependent on the concentration of ferric iron available at the mineral surface, an increase in dissolution rate is anticipated in microbial communities that have a mechanism for the continual oxidation of Fe^{2+} to Fe^{3+} (Wakao et al., 1982; 1984). Our observation of enhanced rates in the presence of iron-oxidizing species can be attributed primarily to the regeneration of ferric iron by the microbial populations in these environments.

4.2. The Role of Sulfur Oxidizers

The most obvious change in surface composition induced by microbial populations is the almost complete absence of elemental sulfur on the surfaces of those samples exposed to the sulfur-oxidizing *T. caldus.* Although marcasite and arsenopyrite samples from the *F. acidarmanus* and enrichment cultures, as well as the abiotic control, all reveal significant amounts of elemental sulfur on the surface, our experiments indicate that little elemental sulfur is present with *T. caldus.* Our results suggest that elemental sulfur is probably continually accumu-

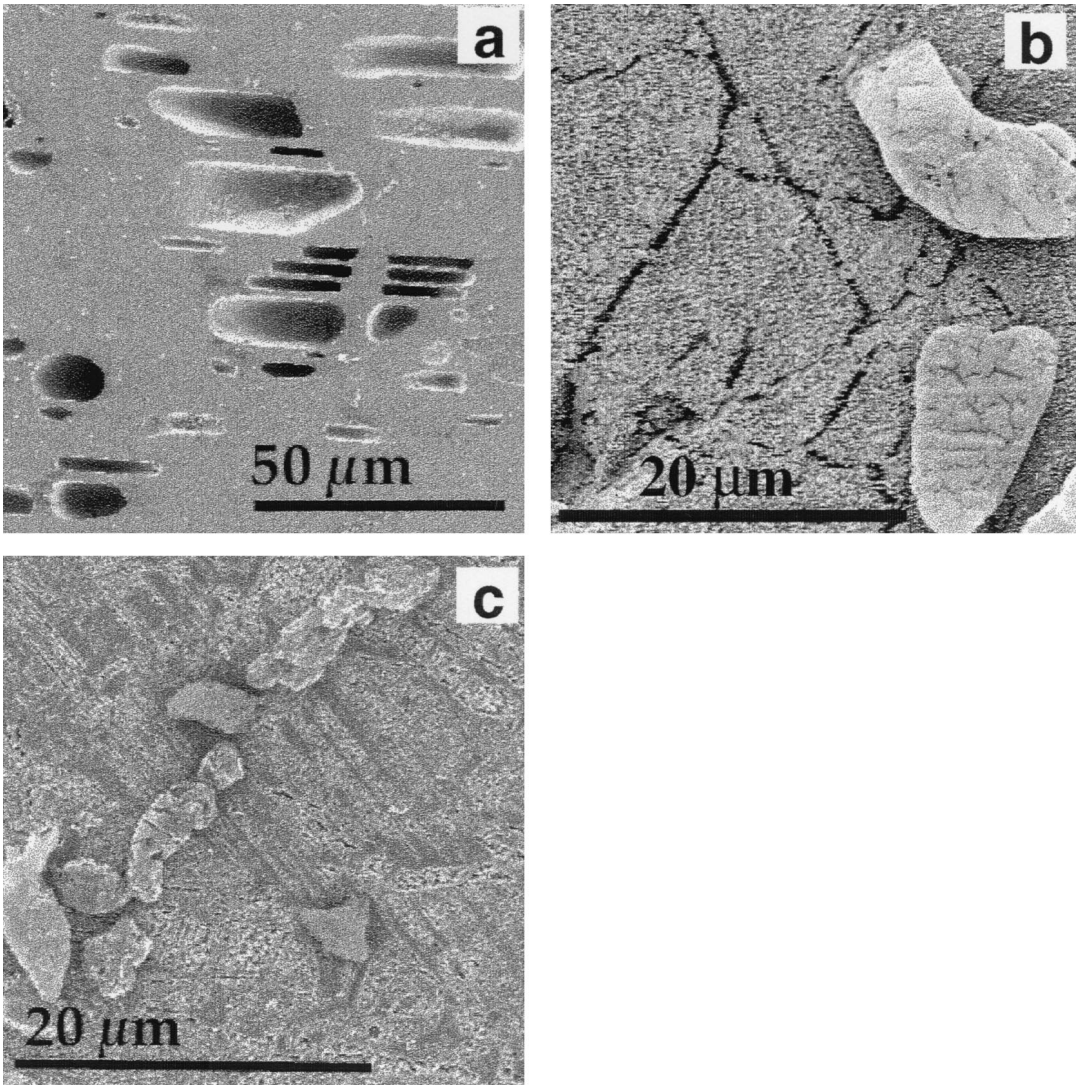

Fig. 10. SEM images of pyrite after 22 days reaction with *F. acidarmanus* (a), marcasite after 22 days reaction with the enrichment culture (b), and arsenopyrite after 22 d reaction with *F. acidarmanus* (c). All reactions were at pH 1.5 and 37°C.

lating on the mineral surface during the oxidation of arsenopyrite and marcasite at low pH. The formation of elemental sulfur is most likely the result of a complex oxidation pathway, probably involving polysulfides as noted previously (Mycroft et al., 1990; Nesbitt and Muir, 1994). In the presence of a sulfur-oxidizing microbial population, however, the sulfur is removed continuously from the mineral surface as it forms.

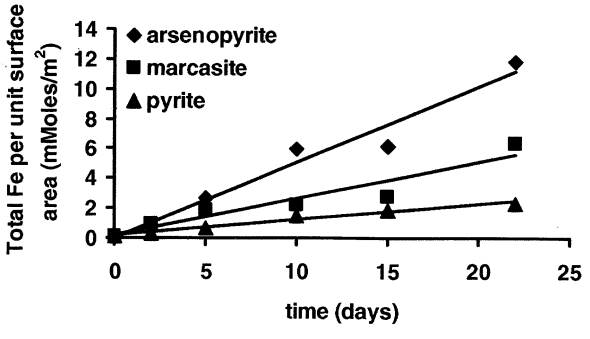

Fig. 11. Total soluble iron concentration vs. time for each of the minerals in the abiotic control media at pH 1.5 and 37°C. The lines represent the best straight-line fit for each data series.

4.3. Mixed Populations of Iron and Sulfur Oxidizers

Although our experiments generally indicate that mineral samples show an increased dissolution rate when exposed to cultures of iron-oxidizing microbes, our measurements reveal that the greatest rate enhancement occurs when the sulfur-oxidizing species *T. caldus* is added to the mixture of the iron-oxidizing species *Leptospirillum ferrooxidans* and *F. acidarmanus.* Because *T. caldus* alone does not increase the rate of dissolution significantly, the additional rate enhancement induced by the mixed enrichment cultures over that induced by the pure *F. acidarmanus* cultures cannot be attributed to a simple additive contribution of the sulfur-oxidizing species. The other difference between the two microbial populations

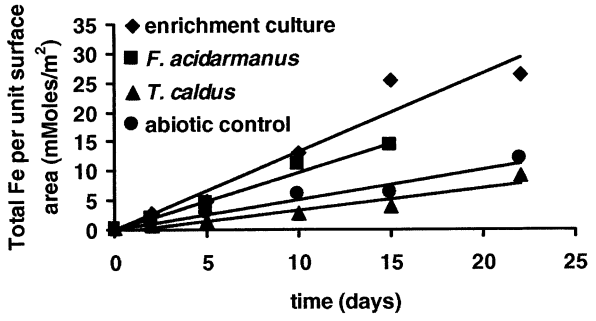

Fig. 12. Total soluble iron concentration vs. time for arsenopyrite in each of the three microbial cultures and the abiotic control. All reactions were at pH 1.5 and 37°C. The lines represent the best straight-line fit for each data series.

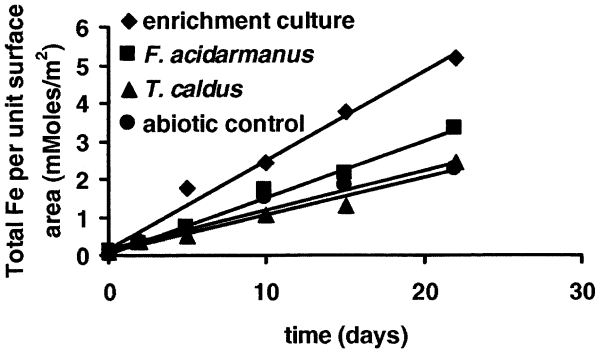

Fig. 14. Total soluble iron concentration vs. time for pyrite in each of the three microbial cultures and the abiotic control. All reactions were at pH 1.5 and 37°C. The lines represent the best straight-line fit for each data series.

was the presence of a second iron-oxidizing species, *L. ferrooxidans,* in the enrichment culture. However, previous studies have shown that the rates of iron oxidation of different species do not vary considerably (Norris, 1990), and therefore, the enhanced rate of dissolution in the enrichment culture is most likely not due to differences in cell-normalized iron oxidation rates between the microbial cultures. In addition, the average cell counts do not indicate significant differences in the size of the iron-oxidizing populations between the *F. acidarmanus* isolate and enrichment cultures. Although it is clear that the presence of iron and sulfur oxidizers together results in an increase in dissolution compared with an iron-oxidizing culture alone, at this time we are unable to establish the basis for this apparent consortia effect.

4.4. Effects of Elemental Sulfur at the Mineral Surface

Understanding the possible influence of insoluble surface products such as elemental sulfur on the dissolution rate is important in developing a more complete model for the kinetics of sulfide mineral dissolution. It has been suggested that a sufficiently impenetrable layer of elemental sulfur might passivate the surface to further oxidation by preventing the passage of oxidants to the surface (Curutchet et al., 1996; Dopson and Lindstrom, 1999; Garcia et al., 1995a;b). However, our results show that accumulation of elemental sulfur does not suppress the dissolution rate, even when the amount of sulfur present is sufficient to create a deposit with an average thickness of hundreds of layers. This is most striking when comparing the rate data for the sulfur-oxidizing *T. caldus* cultures to those of the abiotic controls (neither contained iron-oxidizing species). Although elemental sulfur formed on marcasite and arsenopyrite surfaces in the abiotic control reactions, the dissolution rates observed are approximately the same as those measured in the experiments where the accumulation of elemental sulfur was prevented by the presence of *T. caldus.* If elemental sulfur acts as a passivation layer, we would expect the dissolution rates for marcasite and arsenopyrite in the presence of *T. caldus* to be higher than those of their counterparts in the abiotic control.

We offer two explanations as to why the presence of surface deposits of elemental sulfur fails to passivate the mineral surface. One possibility is that the sulfur is forming in discrete patches, leaving parts of the surface exposed, rather than in one continuous blanket over the surface; a second possibility is that the sulfur is spread uniformly over the surface but remains sufficiently porous that reactants and products can diffuse through the sulfur overlayer.

Although there is a possibility that SEM experiments may alter the mineral surface as discussed above, a qualitative analysis of SEM images supports the notion of a heterogeneous distribution of elemental sulfur, often in the form of discrete patches. A more quantitative analysis reveals that the length scale of appreciable variation on a particular sample is on the order of tens of microns or smaller as evidenced by the small (≈15%) variation in signal intensity observed by the Raman imaging studies on longer length scales (hundreds of microns). On a much different scale, large fluctuations in sulfur coverage are observed between different mineral samples. These varia-

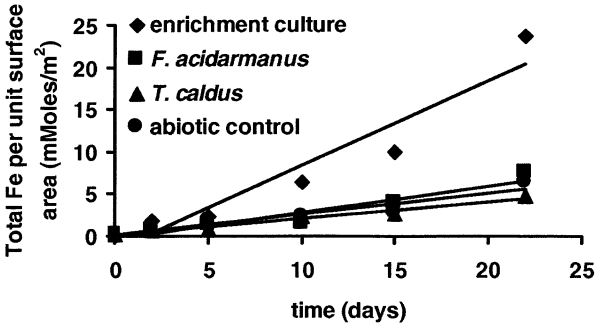

Fig. 13. Total soluble iron concentration vs. time for marcasite in each of the three microbial cultures and the abiotic control. All reactions were at pH 1.5 and 37°C. The lines represent the best straight-line fit for each data series.

Table 3. Average cell counts over the duration of the experiment.

	Pyrite	Marcasite	Arsenopyrite
T. caldus	9×10^8	2×10^9	1×10^9
F. acidarmanus	3×10^9	2×10^9	2×10^9
Enrichment culture: total cells	3×10^9	5×10^9	2×10^9
Enrichment culture: iron oxidizers	2×10^9	3×10^9	1×10^9

tions are most likely due to intrinsic properties of the different samples that may affect their reactivity. Surface features such as step edges, defects, and inclusions that vary from sample to sample are expected to affect the surface chemistry, and the role of such features in the formation of elemental sulfur at the mineral surface warrants further investigation. Indeed, evidence of the heterogeneous nature of the dissolution reactions can be seen in SEM images that reveal patterns of etching that originate at inclusions and site-specific reactivity that results in linear features and localized pits rather than homogeneous dissolution over the entire surface. Although these intrinsic properties of the minerals contribute to differences in surface composition between samples, metabolic differences between microbial populations result in the greatest disparities in surface composition.

5. CONCLUSIONS

It is generally recognized that microbes are able to enhance the dissolution rates of sulfide minerals. Determining the effects of microbial populations on dissolution processes may be extremely complicated if this requires a detailed understanding of the function of each microbe. Our results suggest that, in the laboratory, the ferric ion concentration is the controlling factor in determining the overall dissolution rate. Elemental sulfur deposits do not markedly affect the overall rate because of the inhomogeneous distribution of this reaction product.

Acknowledgments—The authors thank William Ullman for BET measurements and Brian Hess for sample preparation. We also thank Iron Mountain Mine, Inc. for site access and Stauffer Management Co. for providing assistance. This work was supported by grants from the National Science Foundation (CHE 9807598 and CHE 9521731) and the Environmental Protection Agency (R 826189).

Associate editor: E. H. Oelkers

REFERENCES

Arkesteyn G. J. M. W. (1979) Pyrite oxidation by *Thiobacillus ferrooxidans* with special reference to the sulfur moiety of the mineral. *Antonie van Leeuwenhoek.* **45,** 423–435.

Baldi F., Clark T., Pollack S. S., and Olson G. J. (1992) Leaching of pyrites of various reactivities by *Thiobacillus ferrooxidans. Appl. Environ. Microbiol.* **58,** 1853–1856.

Battaglia F., Morin D., and Ollivier P. (1994) Dissolution of cobaltiferous pyrite by *Thiobacillus ferrooxidans* and *Thiobacillus thiooxidans:* Factors influencing bacterial leaching efficiency. *J. Biotechnol.* **32,** 11–16.

Bond P. L., Druschel G. K., and Banfield J. F. (in press) Comparison of acid mine drainage microbial communities in physically and geochemically distinct ecosystems. *Appl. Environ. Microbiol.*

Bond P. L., Smriga S. P., and Banfield J. F. (2000). Phylogeny of microorganisms populating a thick, subaerial, lithotrophic biofilm at an extreme acid mine drainage site. *Appl. Environ. Microbiol.* **66,** 3842–3849.

Buckley A. N. and Walker G. W. (1988) The surface composition of arsenopyrite exposed to oxidizing environments. *Appl. Surf. Sci.* **35,** 227–240.

Chopelas A. (1991) Single crystal Raman spectra of forsterite, fayalite, and monticellite. *Am. Mineral.* **76,** 1101–1109.

Curutchet G., Tedesco P., and Donati E. (1996) Combined degradation of covellite by *Thiobacillus thiooxidans* and *Thiobacillus ferrooxidans. Biotechnol. Lett.* **18,** 1471–1476.

Dawson M. V. and Lyle S. J. (1990) Spectrophotometric determination of iron and cobalt with ferrozine and dithizone. *Talanta.* **37,** 1189–1191.

Dopson M. and Lindstrom E. B. (1999) Potential role of *Thiobacillus caldus* in arsenopyrite bioleaching. *Appl. Environ. Microbiol.* **65,** 36–40.

Edwards K. J., Bond P. L., and Banfield J. F. (2000a). Characteristics of attachment and growth of *Thiobacillus caldus* on sulfide minerals: A chemotactic response to sulfur minerals? *Environ. Microbiol.* **2,** 324–332.

Edwards K. J., Bond P. L., Gihring T. M., and Banfield J. F. (2000b). An archael iron-oxidizing extreme acidophile important in acid mine drainage. *Science* **287,** 1796–1799.

Edwards K. J., Gihring T. M., and Banfield J. F. (1999a) Seasonal variations in microbial populations and environmental conditions at an extreme acid mine drainage environment. *Appl. Environ. Microbiol.* **65,** 3627–3632.

Edwards K. J., Goebel B. M., Rodgers T. M., Schrenk M. O., Gihring T. M., Cardona M. M., Hu B., McGuire M. M., Hamers R. J., Pace N. R., and Banfield J. F. (1999b) Geomicrobiology of pyrite (FeS_2) dissolution: A case study at Iron Mountain, California. *Geomicrobiology* **16,** 155–179.

Edwards K. J., Schrenk M. O., Hamers R. J., and Banfield J. F. (1998) Microbial oxidation of pyrite: Experiments using microorganisms from an extreme acidic environment. *Am. Mineral.* **83,** 1444–1453.

Elsetinow A. R., Guevremont J. M., Strongin D. R., Schoonen M. A. A., and Strongin M. (2000) Oxidation of {100} and {111} surfaces of pyrite: Effects of preparation method. *Am. Mineral.* **85,** 623–626.

Evangelou V. P. and Zhang Y. L. (1995) A review: Pyrite oxidation mechanisms and acid mine drianage prevention. *Crit. Rev. Environ. Sci. Technol.* **25,** 141–199.

Garcia O., Jr, Bigham J. M., and Tuovinen O. H. (1995a) Oxidation of galena by *Thiobacillus ferrooxidans* and *Thiobacillus thiooxidans. Can. J. Microbiol.* **41,** 508–514.

Garcia O., Jr, Bigham J. M., and Tuovinen O. H. (1995b) Sphalerite oxidation by *Thiobacillus ferrooxidans* and *Thiobacillus thiooxidans. Can. J. Microbiol.* **41,** 578–584.

Hirth J. P. and Pound G. M. (1963) *Condensation and Evaporation: Nucleation and Growth Kinetics.* Macmillan.

Kapuscinski J. (1995) DAPI: A DNA-specific fluorescent probe. *Biotechnic. Histochem.* **70,** 220–233.

Lathe R. (1985) Synthetic oligonucleotide probes deduced from amino acid sequence data: Theoretical and practical considerations. *J. Mol. Biol.* **183,** 1–12.

Lizama H. M. and Suzuki I. (1988) Bacteria leaching of a sulfide ore by *Thiobacillus ferrooxidans* and *Thiobacillus thiooxidans.* I. Shake flask studies. *Biotech. Bioeng.* **32,** 110–116.

Lowson R. T. (1982) Aqueous oxidation of pyrite by molecular oxygen. *Chem. Rev.* **82,** 461–497.

McGuire M. M. and Hamers R. J. (in press) Extraction and quantitative analysis of elemental sulfur from sulfide mineral surfaces by high-performance liquid chromatography. *Environ. Sci. Tech.*

McKibben M. A. and Barnes H. L. (1986) Oxidation of pyrite in low temperature acidic solutions: Rate laws and surface textures. *Geochim. Cosmochim. Acta* **50,** 1509–1520.

Mernagh T. P. and Trudu A. G. (1993) A laser microprobe study of some geologically important sulphide minerals. *Chem. Geol.* **103,** 113–127.

Moses C. O., Nordstrom D. K., Herman J. S., and Mills A. L. (1987) Aqueous pyrite oxidation by dissolved oxygen and by ferric iron. *Geochim. Cosmochim. Acta* **51,** 1561–1571.

Mycroft J. R., Bancroft G. M., McIntyre N. S., Lorimer J. W., and Hill I. R. (1990) Detection of sulphur and polysulfides on electrochemically oxidized pyrite surfaces by x-ray photoelectron spectroscopy and Raman spectroscopy. *J. Electroanal. Chem.* **292,** 139–152.

Nesbitt H. W. and Muir I. J. (1994) X-ray photoelectron spectroscopic study of a pristine pyrite surface reacted with water vapour and air. *Geochim. Cosmochim. Acta* **58,** 4667–4679.

Nordstrom D. K. (1982) Aqueous pyrite oxidation and the consequent formation of secondary iron minerals. In *Acid Sulfate Weathering* (eds. J. A. Kittrick, D. S. Fanning, and L. R. Hossner), pp. 37–56. Soil Science Society of America, Madison, WI.

Nordstrom D. K. and Alpers C. N. (1999) Geochemistry of acid mine waters. In *Environmental Geochemistry of Mineral Deposits* (eds.

G. S. Plumlee and M. J. Logsdon), pp. 133–160. Society of Economic Geologists, Littleton, CO.

Nordstrom D. K., Alpers C. N., Ptacek C. J., and Blowes D. W. (2000). Negative pH and extremely acidic mine waters from Iron Mountain, California. *Environ. Sci. Technol.* **34,** 254–258.

Nordstrom D. K. and Southam G. (1997) Geomicrobiology of sulfide mineral oxidation. In *Geomicrobiology: Interactions Between Microbes and Minerals* (eds. J. F. Banfield and K. H. Nealson), pp. 361–390. Mineralogical Society of America, Washington, D.C.

Norris P. R. (1990) Acidophilic bacteria and their activity in mineral sulfide oxidation. In *Microbial Mineral Recovery* (eds. H. L. Erlich and C. L. Brierley), pp. 3–27. McGraw-Hill.

Rinker M. J., Nesbitt H. W., and Pratt A. R. (1997) Marcasite oxidation in low-temperature acidic (pH = 3) solutions: Mechanism and rate laws. *Am. Mineral.* **82,** 900–912.

Sasaki K. (1997) Raman study of the microbially mediated dissolution of pyrite by Thiobacillus ferrooxidans. *Can. Mineral.* **35,** 999–1008.

Sasaki K., Tanaike O., and Konno H. (1998a) Distinction of jarosite-group compounds by Raman spectroscopy. *Can. Mineral.* **36,** 1225–1235.

Sasaki K., Tsunekawa M., Ohtsuka T., and Konno H. (1995) Confirmation of a sulfur-rich layer on pyrite after oxidative dissolution by Fe(III) ions around pH 2. *Geochim. Cosmochim. Acta* **59,** 3155–3158.

Sasaki K., Tsunekawa M., Ohtsuka T., and Konno H. (1998b) The role of sulfur-oxidizing bacteria *Thiobacillus thiooxidans* in pyrite weathering. *Coll. Surf. A.* **133,** 269–278.

Sato S., Higuchi S., and Tanaka S. (1985) Identification and determination of oxygen-containing inorganosulfur compounds by laser Raman spectrometry. *Appl. Spectrosc.* **39,** 822–827.

Schrenk M. O., Edwards K. J., Goodman R. M., Hamers R. J., and Banfield J. F. (1998) Distribution of *Thiobacillus ferrooxidans* and *Leptospirillum ferrooxidans:* Implications for generation of acid mine drainage. *Science* **279,** 1519–1522.

Singer P. C. and Stumm W. (1970) Acidic mine drainage: The rate-determining step. *Science* **167,** 1121–1123.

Thibeau R. J., Brown C. W., and Heidersbach R. H. (1978) Raman spectra of possible corrosion products of iron. *Appl. Spectrosc.* **32,** 532–535.

Turcotte S. B., Benner R. E., Riley A. M., Li J., Wadsworth M. E., and Bodily D. M. (1993) Surface analysis of electrochemically oxidized metal sulfides using Raman spectroscopy. *J. Electroanal. Chem.* **347,** 195–205.

Ushioda S. (1972) Raman scattering from phonons in iron pyrite (FeS^2). *Sol. State Comm.* **10,** 307–310.

Wakao N., Mishina M., Sakurai Y., and Shiota H. (1982) Bacterial pyrite oxidation. 1. The effect of pure and mixed cultures of *Thiobacillus ferrooxidans* and *Thiobacillus thiooxidans* on release of iron. *J. Gen. Appl. Microbiol.* **28,** 331–343.

Wakao N., Mishina M., Sakurai Y., and Shiota H. (1984) Bacterial pyrite oxidation. III. Adsorption of *Thiobacillus ferrooxidans* cells on solid surfaces and its effect on iron release from pyrite. *J. Gen. Appl. Microbiol.* **30,** 63–77.